nanomaterials

MDPI

Article

Synthesis, Characterization, and Antibacterial Activity of Ag_2O-Loaded Polyethylene Terephthalate Fabric via Ultrasonic Method

Armin Rajabi [1,*], Mariyam Jameelah Ghazali [1,*], Ebrahim Mahmoudi [2], Amir Hossein Baghdadi [1], Abdul Wahab Mohammad [2], Nadia Mohd Mustafah [3], Htwe Ohnmar [4] and Amaramalar Selvi Naicker [4]

1 Centre for Materials Engineering and Smart Manufacturing, Faculty of Engineering and Built Environment, Universiti Kebangsaan Malaysia, 43600 UKM Bangi, Selangor, Malaysia; baghdadi.amirhossein@gmail.com
2 Department of Chemical and Process Engineering, Faculty of Engineering and Built Environment, Universiti Kebangsaan Malaysia, 43600 UKM Bangi, Selangor, Malaysia; ebi.dream@gmail.com (E.M.); wahabm@eng.ukm.my (A.W.M.)
3 Department of Rehabilitation Medicine, Faculty of Medicine, Universiti Teknologi MARA, 47000 Sg. Buloh, Selangor, Malaysia; nadiamustafah@gmail.com
4 Rehabilitation Medicine Unit, Department of Orthopaedics & Traumatology, Faculty of Medicine, University Kebangsaan Malaysia, 56000 Cheras, Kuala Lumpur, Malaysia; htwe.om@gmail.com (H.O.); asnaicker@yahoo.com (A.S.N.)
* Correspondence: arminukm50@siswa.ukm.edu.my (A.R.); mariyam@ukm.edu.my (M.J.G.)

Received: 1 January 2019; Accepted: 22 February 2019; Published: 18 March 2019

Abstract: In this study, Ag_2O was synthesized on polyethylene terephthalate fabrics by using an ultrasonic technique with Ag ion reduction in an aqueous solution. The effects of pH on the microstructure and antibacterial properties of the fabrics were evaluated. X-ray diffraction confirmed the presence of Ag_2O on the fabrics. The fabrics were characterized by Fourier transform infrared spectroscopy, ultraviolet–visible spectroscopy, and wettability testing. Field-emission scanning electron microscopy verified that the change of pH altered the microstructure of the materials. Moreover, the antibacterial activity of the fabrics against *Escherichia coli* was related to the morphology of Ag_2O particles. Thus, the surface structure of Ag_2O particles may be a key factor of the antibacterial activity.

Keywords: ultrasonic synthesis; Ag_2O; morphology; polyethylene terephthalate (PET) fabric; inhibition zone

1. Introduction

At present, microbial contamination in healthcare facilities, especially in hospitals, has caused considerable concern among people. Infectious diseases have become a critically important global healthcare problem, which may cause excessive loss of money and human lives [1,2]. Textile materials have become the main base of cross infections in hospitals and medical institutions with the increasing occurrences of antibiotic-resistant bacterial strains and community-type outbreaks. Polyethylene terephthalate (PET) can be utilized as a reusable protective textile in hospitals due to its excellent mechanical properties, such as thermal stability, durability and reusability, ease of processing, and cost-effectiveness [3,4]. The production and consumption of reusable PET in medical applications, such as lab coats and privacy drapes, have constantly increased in recent years due to the increase in demand for reusable textiles. However, PET is vulnerable to contamination of many microorganisms, such as viruses, bacteria, and spores; some of these may survive for approximately

90 days on PET [5,6]. Thus, contaminated PET can serve as an important medium for infectious diseases. For this reason, effective and generable antimicrobial PET fabrics should be investigated and developed. At present, nanoparticles (NPs) have been recognized as improving antibacterial activity and have attracted considerable attention from scholars in their applications, such as clothing, wound dressings, food packaging, cosmetics, and dental restorative materials [7–9]. On this basis, PET textures treated with antimicrobial agents have been generally investigated and the results have shown its capacity to halt the development of pathogenic microorganisms, such as parasites and microscopic organisms [10,11]. Antimicrobial NPs present many unique benefits compared with popular antibacterial agents. These benefits include cost-effectiveness and overcoming resistance [12]. Several antimicrobial agents (zinc, copper, and silver) have been utilized as antimicrobial varnishes on fabric materials [13–15]. Among the previously mentioned antibacterial materials, silver nano-oxide has been extensively used on cotton and artificial fibers, such as thin polymer films, wound pads, polyester, and drinking water-related applications [16,17]. Notably, the antimicrobial nature of nano-Ag_2O has been widely recognized due to its wide spectrum killing and moderately low risk to microbial resistance development [18,19]. Silver's antibacterial properties are due to its high valence state which causes strong electrostatic attractions between the Ag ion and bacteria [14,20,21]. The antimicrobial activity of metallic NPs is recognized to be remarkably influenced by their shape and size, which are largely affected by preparation procedures. Several matters occur in the synthesis of NP-coated fabrics. The remaining matters are those with expensive and advanced equipment requirements and the difficulties of control methodology.

Ultrasonication is an effective method used to synthesize inorganic materials, counting metals, and metal oxides [22,23]. Sonochemistry is derived from acoustic cavitation, which is the creation, growth, and implosive collapse of bubbles within a liquid. Acoustic cavitation is the main mechanism following the sonochemical synthesis of nanomaterials. The development and collapse of bubbles inside the solution are related to the applied ultrasound frequency [24,25]. Other benefits of sonochemical synthesis include convenience, environmental-friendliness, rapidity instead of fast processes, and effectiveness [26,27]. Jimmy et al. [28] have reported that photocatalytically active TiO_2 NPs synthesized through an ultrasonic method are more profitable than that of commercial NPs, owing to the improved oxide crystallinity with fast hydrolysis rate by ultrasound. On this basis, a high-intensity (30 kHz) ultrasound sonochemical method has been used to synthesize and recognize novel nanomaterials without using high temperatures and long reaction times [29].

However, only a few studies have focused on the synthesis of Ag_2O nanomaterials by using an ultrasonic technique. This study aimed to synthesize Ag_2O nano-loaded PET fabrics under various pH by using an ultrasonic method and to characterize the microstructure and antibacterial behavior of the fabrics.

2. Materials and Methods

$AgNO_3$ (99% *w*/*w*) and NaOH pellets (98% *w*/*w*) were obtained from a local brand company (R&M, Semenyih, Malaysia). One mole of $AgNO_3$ was dissolved in deionized water under magnetic stirring for 15 min at room temperature and pH solution was adjusted by sodium hydroxide (Table 1). PETs 5 mm in diameter were obtained from a local brand, washed with distilled water, and dried in an air oven at 70 °C for 12 h. PETs were soaked in the solutions for 5 h and were mildly stirred at 25 °C. The mixture consisted of aqueous solution and PETs were sonicated (30 kHz) for 15 min. PETs were removed from the solution, washed with distilled water, and dried in an oven at 70 °C for 12 h. X-ray diffraction (XRD) analysis was conducted on PETs using a Bruker AXS (GmbH Oestliche Rheinbrueckenstr, Karlsruhe, Germany) diffractometer with monochromatic Cu–Kα radiation (λ = 0.1541 nm) at 4 mA and 40 kV. A Perkin–Elmer Spectrum 400 Fourier transform infrared (FTIR/FTNIR) spectroscope (Akron, OH, USA) was used to evaluate the chemical composition of the samples in the region 500–4000 cm^{-1}. The UV–Vis absorption properties of the samples were evaluated through absorption spectroscopy using a Perkin–Elmer Lambda-35 UV–Vis spectrophotometer. Prior

to electron microscopy, the samples were coated with a thin layer of iridium to avoid the charging effect instigated by the non-conductive property of the fabrics. The morphological behavior and contact angle (CA) of the samples were assessed using a field emission scanning electron microscope (FESEM; Zeiss Merlin, Zurich, Switzerland) and an optical tensiometer (Theta of Attension, Biolin Scientific, Hängpilsgatan, Västra Frölunda, Sweden). Disk diffusion antibiotic sensitivity testing (Kirby–Bauer antibiotic testing) was employed to evaluate the efficiency of PETs against *Escherichia coli*. Firstly, fabrics embedded with nanoparticles at different pH were a cut as disks with a diameter of 0.5 mm. Then, 30 µL of *E. coli* solution (nutrient broth Himedia M001, West Chester, PA, USA) with a concentration of 16×10^7 cells/mL (OD600 of 0.2) was spread on a petri dish containing nutrient agar (Himedia M002, West Chester, PA, USA). The fabric discs containing Ag2O nanomaterial were placed on each Petri dish and a piece of uncoated fabric was used as a control in each set of tests. The Petri dishes were incubated at 35 °C for 24 h, digital images of the plates were captured, and the inhibition zone was calculated using an image processing software (image J.140, University of Wisconsin, Madison, WI, USA) [20,30]; each test was repeated three times and the average results were reported.

Table 1. Sample label with different pH. Legend: PET, polyethylene terephthalate.

Sample Label	Description
F1	Ag_2O-coated PET fabric synthesized at pH 6.5
F2	Ag_2O-coated PET fabric synthesized at pH 7.5
F3	Ag_2O-coated PET fabric synthesized at pH 8.5
F4	Ag_2O-coated PET fabric synthesized at pH 9.5
F5	Ag_2O-coated PET fabric synthesized at pH 10.5

3. Results and Discussion

3.1. X-ray Diffraction Analysis

The XRD results of presence and purity of Ag_2O crystalline grown on the surface of PETs are shown in Figure 1. As shown in Figure 1, the characteristic peaks of a crystalline PET structure in the fabric appeared at peaks $2\theta = 16°$, 22°, and 26° for the original and coated fabrics. However, Ag_2O-PET fabric samples showed characteristic diffraction peaks of Ag_2O at $2\theta = 26.9°$, 32.69°, 37.94°, 54.9°, 65.54° and 69°, which agrees with silver (I) oxide FCC crystalline phase (JCPDS 041-1104). Meanwhile, these Ag_2O peaks were clearly absent in the F1 sample due to the low quantity of materials, as previously reported for other materials [20,31]. Furthermore, no strange diffraction peaks were detected in the XRD patterns of all Ag_2O-coated fabric samples, which confirms the existence of the high crystalline quality of the Ag_2O-coated fabric surface. For the main diffraction peak ($2\theta = 32.69°$), the full width at half maximum (FWHM) became sharp and narrow for the F3, F4, and F5 samples, where the values are 0.4379075°, 0.4278235°, and 0.4119844°, respectively, which shows the increase in the crystallinity of Ag_2O nanoparticles for the F4 and F5 samples with an increase in pH. The average crystalline sizes of Ag_2O NPs at different pH (6.5, 7.5, 8.5, 9.5, and 10.5) were calculated using Scherrer's equation [31,32] and were found to be 19.23 nm, 20.65 nm, 18.91 nm, 19.35 nm, and 21 nm, respectively. The crystalline size of the materials moderately increased from F4 into F5 and reached the maximum value with the highest pH. However, the decrease in crystalline size of Ag_2O NPs for F3 was confirmed by the inhibition of peak intensity and increase of FWHM. The increment in the crystalline size was due to high nucleation rate and growth of Ag_2O nanocrystallites with the accessibility of sufficient thermal energy due to high NaOH concentration in the precursor, as has been reported in a previous works [20,33].

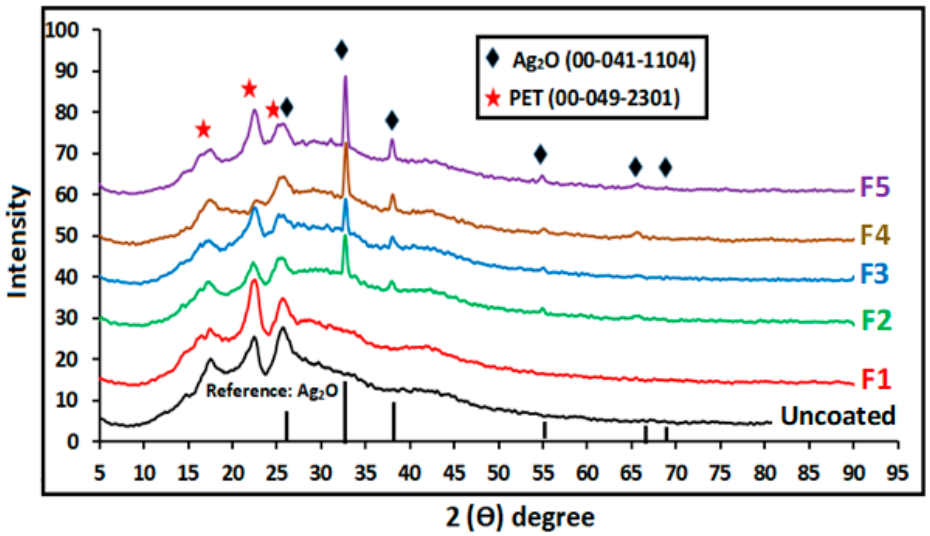

Figure 1. X-ray diffraction (XRD) patterns of synthesized Ag_2O with different pH.

3.2. Microstructural Observation

The size and morphology of PET fabrics after Ag_2O coating can be clearly observed at two different magnification sizes, as shown in Figure 2. The microstructures of the synthesized materials at low magnification are similar and agglomeration particles can be observed. Although the growth mechanism of Ag_2O is difficult to determine, the details for the formation of different particle sizes may be explained based on the literature [34,35]. In acid solution (pH = 6.5), a small particle of nano-sized Ag_2O on the PET surface was observed, as shown in Figure 2a by the yellow circle. This condition was ascribed to the etching in acidic solution. The concentration of H^+ ions increases the reaction with OH^- on the surface of the Ag^+ precursor and remarkably inhibits the growth of Ag_2O. However, the yellow circle (Figure 2b) reveals a starfish-like morphology at high magnification, which is composed of a series of regular rod shapes in the range of 200–4500 nm and 160–200 nm for length and width, respectively. Notably, the effect of H^+ ions is inferior, and Ag_2O particles start growing from the Ag^+ precursor at high pH. Therefore, the role of pH can be crucial in controlling the size and shape of NPs. Figure 2d (pH = 7.5) at high magnification shows that the powder morphology involves a large amount of semiregular spherical particles with sizes in the range of 100–400 nm. Cavitation bubbles were generated and oscillated with high frequency with the introduction of ultrasound [36,37]. The oscillation of cavitation bubbles fragmented the microstructure of the rods into small grains and were moved by acoustic streaming. Most recently, sonofragmentation of particles by a shock wave has been added to the effects of a shock wave created by ultrasound irradiation. Zeiger et al. [38] have successfully eliminated many possible mechanisms of particle breakage, such as particle–particle, particle–horn, and particle–wall collisions through kinetics. Consequently, they inferred breakage by a particle shock wave interaction as a viable mechanism for the sonofragmentation of acetylsalicylic acid. In this study, particles dispersed in the liquid phase, stuck to one another, and formed an agglomerate structure, which resulted in poor access to the constituent rod-like particles in the powders (Figure 2d). The microstructure of the powders at pH = 8.5 consisted of two different morphologies, namely, semiregular spherical and rod-shaped particles (Figure 2f). The growth mechanism of the Ag_2O rod-shaped particles was not known at this stage. However, sonication irradiation at pH = 8.5 facilitated the incorporation of rod-shaped-inducing fragmented rods (nucleation sites) into semiregular spherical and inducing rod-shaped particles (F3). In fact, ultrasound-induced interparticle collisions led to a considerable enhancement of intergrain coupling. Notably, the moderate change from rod-shaped particles to semiregular spherical particles was observed in the morphology in Figure 2h. However, the rod-shaped particles were shortened to semi-spherical due to their lower Gibbs free energy and became homogenously dispersed, as shown in Figure 2j.

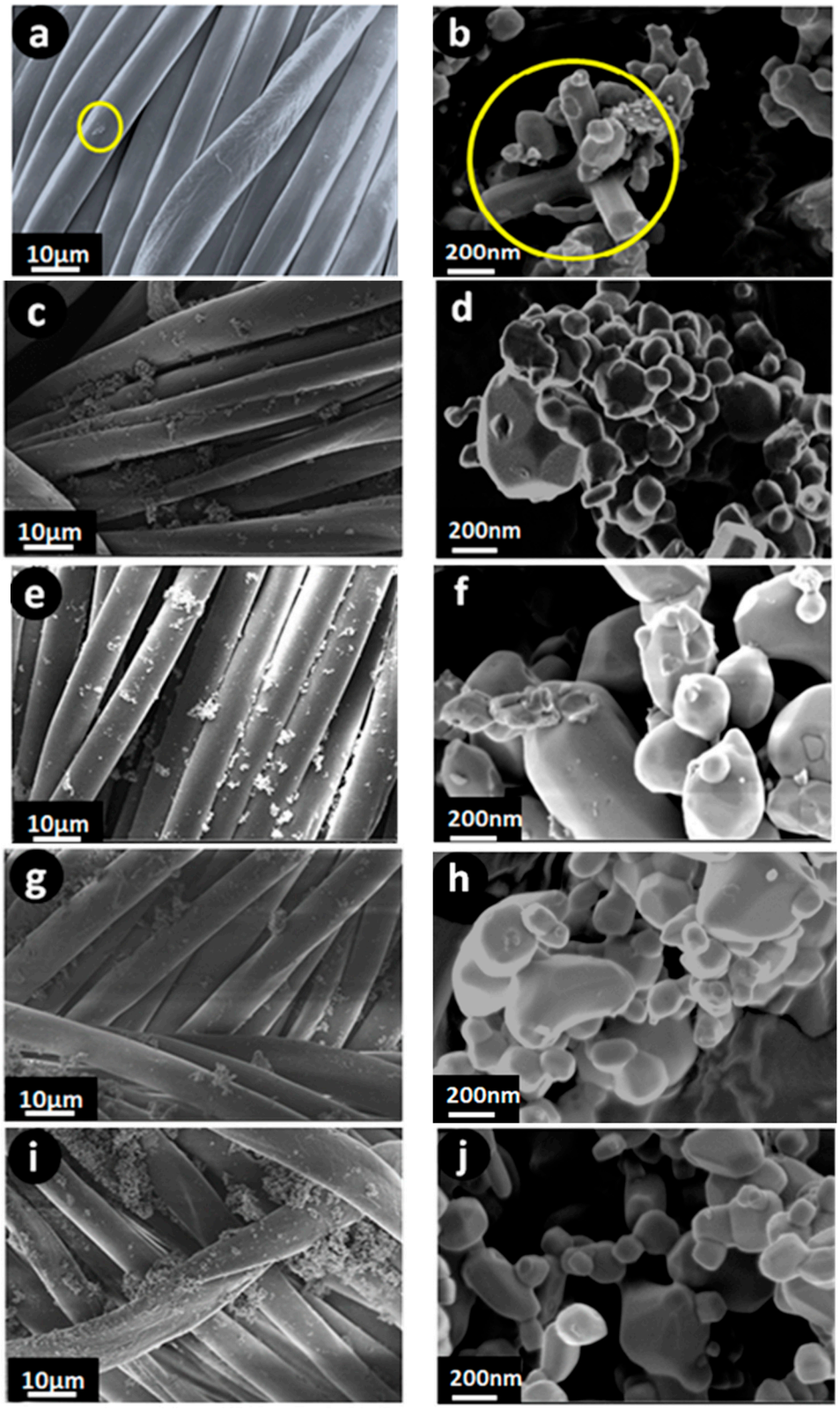

Figure 2. *Cont*.

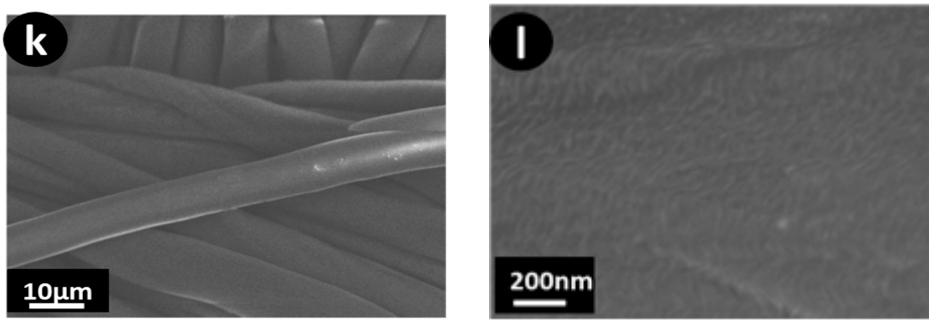

Figure 2. Field emission scanning electron microscope (FESEM) images of the samples at different magnifications. (**a**,**b**) F1, (**c**,**d**) F2, (**e**,**f**) F3, (**g**,**h**) F4, (**i**,**j**) F5, and (**k**,**l**) uncoated.

3.3. FTIR Results

FTIR has become a popular method used to obtain data on functional groups. The FTIR spectra in the 500–4000 cm^{-1} region of the original PET and Ag_2O-coated fabrics are displayed in Figure 3. FTIR shows two regions, namely, the functional group (4000–1504 cm^{-1}) and fingerprint regions (1504–500 cm^{-1}). As shown in Figure 3, all the functional groups of the original PET and Ag_2O-coated fabrics are similar. Therefore, the main structure of the materials is the same. The summary of infrared vibration is represented in Table 2 [39–41]. Although the transmittance spectra appear relatively similar to each other, a decrease in the intensity of the F3 sample can be observed, which is attributed to particle size/morphology, as discussed in the FESEM image (Figure 2).

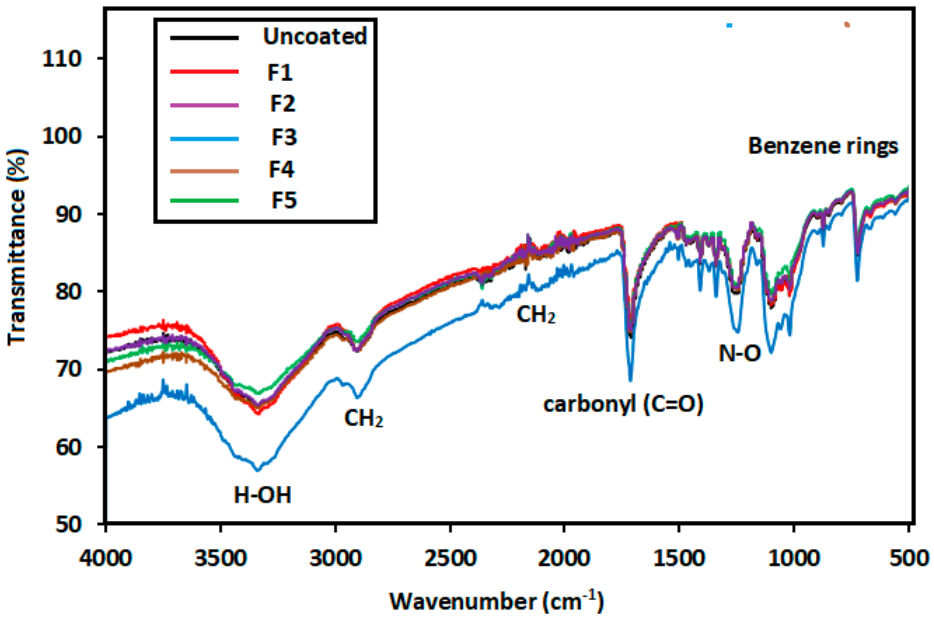

Figure 3. Fourier transform infrared (FTIR) spectra of the samples at different pH.

Table 2. Infrared vibration from FTIR analysis.

Wavenumber (cm^{-1})	Vibration Characteristics	Wavenumber (cm^{-1})	Vibration Characteristics
3339	–H bonded OH stretch	1339	N–O stretching
2874	C–H_2 groups	1247	C–O) vibrations
2361	C–H_2 groups	1098	(C–O) vibrations
1712	carbonyl (C=O) stretching	1018	(C–O) vibrations
1560	phenyl groups	650–900	benzene rings
1408	methylene groups		

3.4. UV–Vis Tests

Figure 4 displays the UV–Vis absorption spectrum of the obtained samples at different pH. The maximum peak of PET shifted to left with Ag_2O loading, which verifies the existence of Ag_2O on the fabric (F2, F3, F4, and F5), as shown in the XRD results. The low peak intensity in the F2 sample (236 nm) may be due to low quantity of Ag_2O, as discussed in the XRD results (Figure 1). Furthermore, a sharp absorption band was noted at 237 nm, 235 nm, 234 nm, 232 nm, and 230 nm for the Ag_2O-loaded fabric at different pH values of 8.5, 9.5, 10.5, 7.5, and 6.5, respectively. The increased absorption of the samples at pH = 8.5 compared with the rest is due to the rod morphology of NPs, as shown in the FESEM images (Figure 2). Rokade et al. [42] have reported that the change of absorption bands is related to morphology of particles, such as Ag_2O nanopowders.

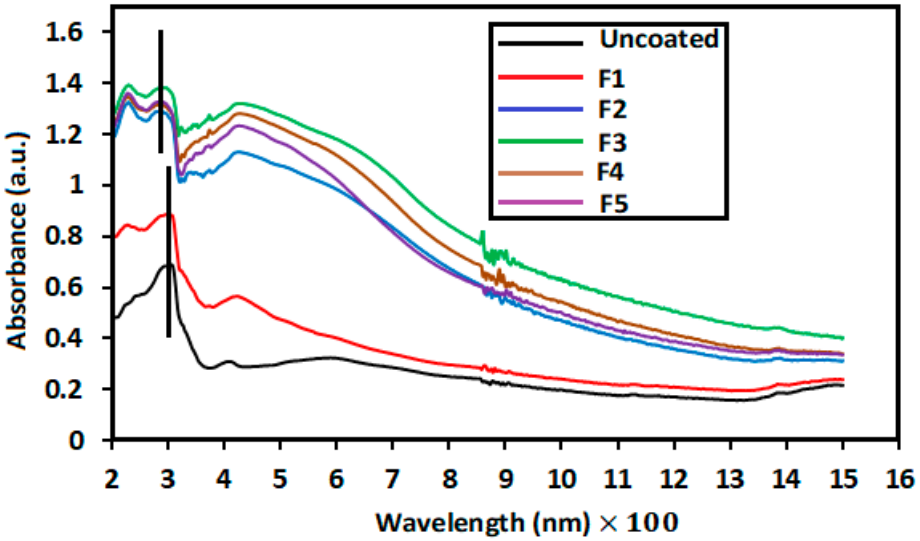

Figure 4. UV–Vis absorbance spectra of the samples.

3.5. Wettability Results

Hydrophobicity and hydrophilicity of materials, that is, surfaces with contact angles (CA) higher and lower than 65°, respectively, have been obtained based on captured photos and contact angle measurements of 1 mL water droplets as a quantitative method [20,43]. Based on the literature [44,45], surface energy and surface roughness are the main factors used to control the CA. Therefore, wettability of the surfaces is changed based on the modifications of roughness and morphology of microstructures. A typical PET fabric can be completely wetted by water droplets (Figure 5a) due to the presence of hydrophilic –OH groups, as illustrated in Table 2. The loading of Ag_2O particles onto the fabric could make the fabric rough and hydrophobicity would be introduced to the PET fabric. Here, the average CA values of PET-loaded Ag_2O at different pH values (6.5, 7.5, 8.5, 9.5 and 10.5) were 95.2°, 94.1°, 122.1°, 94.8° and 96.9°, respectively, and uncoated had a value of ~0° (Figure 5). As shown in Figure 5, the F3 sample exhibits high CA and is more hydrophobic than other samples, which confirms that the surface was successfully modified and has obtained a self-cleaning condition. Therefore, high hydrophobicity (CA of approximately 122.1° similar to Teflon coating [46]) of the PET fabric can exhibit good self-cleaning, and is highlighted as a promising candidate for antibacterial activity. Suryaprabha et al. [47] have reported that the self-cleaning and antibacterial properties of fabrics are improved with an increase in CA.

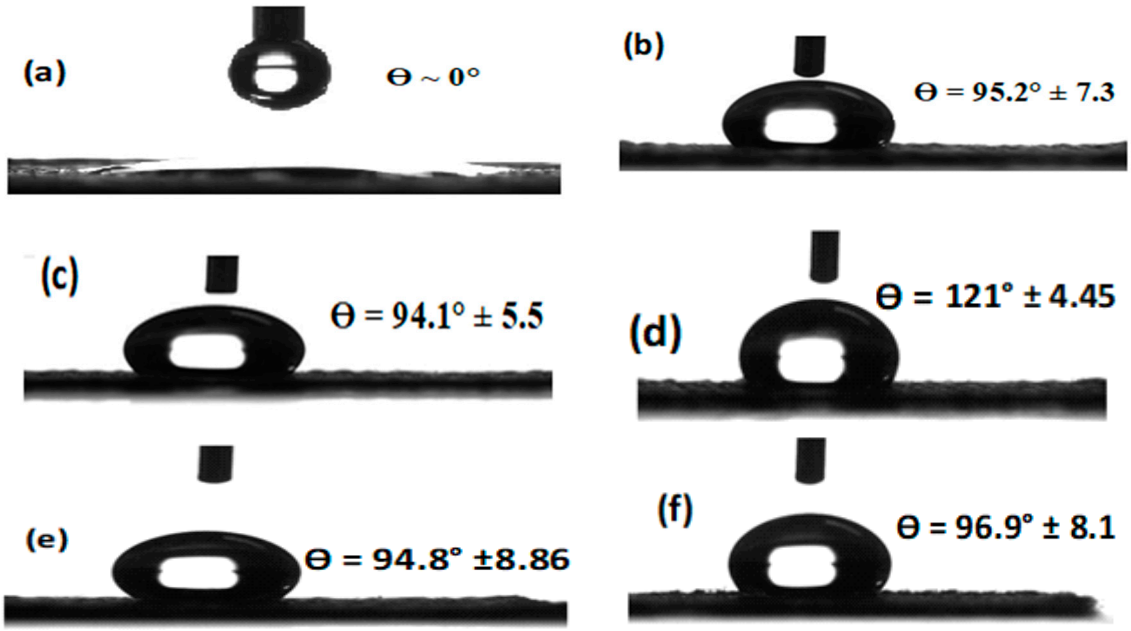

Figure 5. Contact angle of the samples. (**a**) Uncoated, (**b**) F1, (**c**) F2, (**d**) F3, (**e**) F4, and (**f**) (F5).

3.6. Antibacterial Tests

The inhibition zone of the obtained PET-loaded Ag_2O against *E. coli* is shown in Figure 6, and the values are given in Table 3. The diameter of the inhibition zone of the F3 sample is higher than that of other samples. This result suggests that the F3 sample with nanorod morphology exhibits a remarkable growth inhibitory effect against *E. coli*. The results of the present study are similar to results reported by other researchers [20,48,49]. The observed good antibacterial activity is attributed to (a) the large surface area of Ag_2O nanorods as seen in FESEM analysis and (b) the high absorption behavior of Ag_2O nanorods as seen in UV tests. The possible mechanisms for the antibacterial activity of Ag_2O are expressed as follows: (i) Ag_2O contacts and penetrates bacterial cells due to its nanometre scale and rod-like morphology. DNA misses its repetition capability when bacteria are subjected to Ag_2O NPs. Cells are influenced by oxidative stress, which is caused by the inhibition of ATP synthesis [50,51] (the energy currency of cells for all organisms) and occurrence of reactive oxygen species (ROS) [20,52]. ROS increases with the increase in surface area and appropriate crystal sizes. XRD results illustrate that the crystalline size of F3 is 18.91 nm, which can support antibacterial activity. (ii) After the penetration of nanomaterials, the bacterial enzymes deactivate by releasing atomic Ag^0 and ionic Ag^+ clusters, which kill the bacterial cells and increase the inhibition zone [53,54].

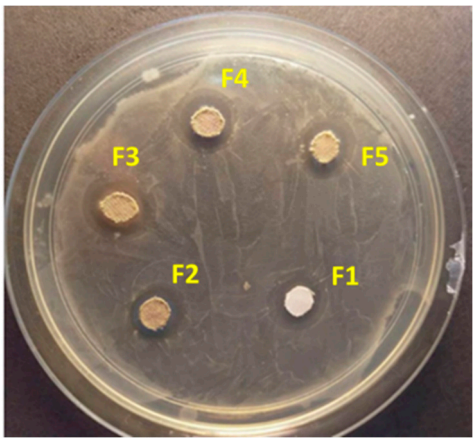

Figure 6. Antibacterial activity of Ag_2O-loaded PETs.

Table 3. Antibacterial activity of the samples.

Sample Label	Inhibition Zone Diameter (mm)
F1	11 ± 0.3
F2	13 ± 0.1
F3	14 ± 0.2
F4	12 ± 0.3
F5	11 ± 0.3

4. Conclusions

In this study, Ag_2O-loaded PET fabrics were successfully synthesized using an ultrasonic method with $AgNO_3$ as a precursor solution. The morphology, CA, and antibacterial activity of the fabrics were dependent on the change of pH. A sharp band at 237 nm in the UV test with the lowest transmittance in the FTIR results was observed at pH 8.5 with nanorod morphology, as shown by FESEM analysis. Furthermore, the antibacterial results revealed a direct relationship with morphology. Thus, the maximum inhibition zone obtained for the fabrics was 14 ± 2 mm because of the large surface area of the Ag_2O nanorods. The results of this study may be applicable to medical devices that are coated with Ag_2O nanorods via ultrasonic methods to improve antibacterial activity.

Author Contributions: A.R. conceived of the presented idea. M.J.G. and A.W.M. were involved in planning and supervised the work. A.R., E.M., and A.H.B. processed the experimental data, performed the analysis, drafted the manuscript and designed the figures. N.M.M., H.O., and A.S.N. contributed to the interpretation of the results. All authors discussed the results and commented on the manuscript.

Funding: This research was funded by Universiti Kebangsaan Malaysia (UKM) under grant number AP-2017-008/5 and MI-2017-002.

Acknowledgments: The author wishes to acknowledge the financial support provided by Universiti Kebangsaan Malaysia (UKM) or the National University of Malaysia for this project under AP-2017-008/5 and MI-2017-002.

Conflicts of Interest: The authors declare no conflict of interest. The funders had no role in the design of the study; in the collection, analyses, or interpretation of data; in the writing of the manuscript, or in the decision to publish the results.

References

1. Giavaresi, G.; Meani, E.; Sartori, M.; Ferrari, A.; Bellini, D.; Sacchetta, A.C.; Meraner, J.; Sambri, A.; Vocale, C.; Sambri, V. Efficacy of antibacterial-loaded coating in an in vivo model of acutely highly contaminated implant. *Int. Orthop.* **2014**, *38*, 1505–1512. [CrossRef] [PubMed]
2. Russotto, V.; Cortegiani, A.; Raineri, S.M.; Giarratano, A. Bacterial contamination of inanimate surfaces and equipment in the intensive care unit. *J. Intensive Care* **2015**, *3*, 54. [CrossRef]
3. Montazer, M.; Shamei, A.; Alimohammadi, F. Stabilized nanosilver loaded nylon knitted fabric using BTCA without yellowing. *Prog. Org. Coat.* **2012**, *74*, 270–276. [CrossRef]
4. Wang, M.; Zhang, M.; Pang, L.; Yang, C.; Zhang, Y.; Hu, J.; Wu, G. Fabrication of highly durable polysiloxane-zinc oxide (ZnO) coated polyethylene terephthalate (PET) fabric with improved ultraviolet resistance, hydrophobicity, and thermal resistance. *J. Colloid Interf. Sci.* **2019**, *537*, 91–100. [CrossRef]
5. Neely, A.N.; Orloff, M.M. Survival of some medically important fungi on hospital fabrics and plastics. *J. Clin. Microbiol.* **2001**, *39*, 3360–3361. [CrossRef] [PubMed]
6. Neely, A.N.; Maley, M.P. Survival of enterococci and staphylococci on hospital fabrics and plastic. *J. Clin. Microbiol.* **2000**, *38*, 724–726.
7. Augustine, R.; Kalarikkal, N.; Thomas, S. Electrospun PCL membranes incorporated with biosynthesized silver nanoparticles as antibacterial wound dressings. *Appl. Nanosci.* **2016**, *6*, 337–344. [CrossRef]
8. Lim, J.P.; Baeg, G.H.; Srinivasan, D.K.; Dheen, S.T.; Bay, B.H. Potential adverse effects of engineered nanomaterials commonly used in food on the miRNome. *Food Chem. Toxicol.* **2017**, *109*, 771–779. [CrossRef]
9. Jemat, A.; Ghazali, M.; Razali, M.; Otsuka, Y.; Rajabi, A. Effects of TiO2 on microstructural, mechanical properties and in-vitro bioactivity of plasma sprayed yttria stabilised zirconia coatings for dental application. *Ceram. Int.* **2018**, *44*, 4271–4281. [CrossRef]

10. Zhu, Y.; Wang, Y.; Sha, L.; Zhao, J. Preparation of antimicrobial fabric using magnesium-based PET masterbatch. *Appl. Surf. Sci.* **2017**, *425*, 1101–1110. [CrossRef]
11. Shahidi, S.; Moazzenchi, B. The Influence of Dyeing on the Adsorption of Silver and Copper Particles as Antibacterial Agents on to Cotton Fabrics. *J. Nat. Fibers* **2018**, 1–11. [CrossRef]
12. Pelgrift, R.Y.; Friedman, A.J. Nanotechnology as a therapeutic tool to combat microbial resistance. *Adv. Drug Deliv. Rev.* **2013**, *65*, 1803–1815. [CrossRef] [PubMed]
13. Malachová, K.; Praus, P.; Rybková, Z.; Kozák, O. Antibacterial and antifungal activities of silver, copper and zinc montmorillonites. *Appl. Clay Sci.* **2011**, *53*, 642–645. [CrossRef]
14. Eremenko, A.; Petrik, I.; Smirnova, N.; Rudenko, A.; Marikvas, Y. Antibacterial and antimycotic activity of cotton fabrics, impregnated with silver and binary silver/copper nanoparticles. *Nano. Res. Lett.* **2016**, *11*, 28. [CrossRef] [PubMed]
15. Mahmoudi, E.; Ang, W.L.; Ng, C.Y.; Ng, L.Y.; Mohammad, A.W.; Benamor, A. Distinguishing characteristics and usability of graphene oxide based on different sources of graphite feedstock. *J. Colloid Interf. Sci.* **2019**, *542*, 429–440. [CrossRef] [PubMed]
16. Zhang, Y.; Xu, Q.; Fu, F.; Liu, X. Durable antimicrobial cotton textiles modified with inorganic nanoparticles. *Cellulose* **2016**, *23*, 2791–2808. [CrossRef]
17. Pal, A.; Sung, B.; Prasad, B.A.B.; Schuber, P.T.; Prasad, S.; Aggarwal, B.B.; Bornmann, W.G. Curcumin glucuronides: Assessing the proliferative activity against human cell lines. *Bioorg. Med. Chem.* **2014**, *22*, 435–439. [CrossRef]
18. Tian, H.; Zhang, Z.-Y.; Liu, C.-Y. Construction of needle-like crystalline AgO ordered structures from Ag nanoparticles and their properties. *New J. Chem.* **2018**, *42*, 5376–5381. [CrossRef]
19. Yoo, J.-Y.; Jang, E.-Y.; Jeong, S.-Y.; Hwang, D.-Y.; Son, H.-J. Bacterial indoleacetic acid-induced synthesis of colloidal Ag_2O nanocrystals and their biological activities. *Bioprocess Biosyst. Eng.* **2018**, 1–14. [CrossRef]
20. Rajabi, A.; Ghazali, M.J.; Mahmoudi, E.; Azizkhani, S.; Sulaiman, N.; Mohammad, A.; Mustafah, N.M.; Ohnmar, H.; Naicker, A. Development and antibacterial application of nanocomposites: Effects of molar ratio on Ag_2O–CuO nanocomposite synthesised via the microwave-assisted route. *Ceram. Int.* **2018**, *44*, 21591–21598. [CrossRef]
21. Mahmoudi, E.; Ng, L.Y.; Ang, W.L.; Chung, Y.T.; Rohani, R.; Mohammad, A.W. Enhancing Morphology and Separation Performance of Polyamide 6, 6 Membranes By Minimal Incorporation of Silver Decorated Graphene Oxide Nanoparticles. *Sci. Rep.* **2019**, *9*, 1216. [CrossRef] [PubMed]
22. Sasidharan, M.; Nakashima, K. Core–shell–corona polymeric micelles as a versatile template for synthesis of inorganic hollow nanospheres. *Accounts Chem. Res.* **2013**, *47*, 157–167. [CrossRef] [PubMed]
23. Anandan, S.; Lee, G.-J.; Wu, J.J. Sonochemical synthesis of CuO nanostructures with different morphology. *Ultrason. Sonochem.* **2012**, *19*, 682–686. [CrossRef] [PubMed]
24. Bang, J.H.; Suslick, K.S. Applications of ultrasound to the synthesis of nanostructured materials. *Adv. Mater.* **2010**, *22*, 1039–1059. [CrossRef]
25. Xu, H.; Zeiger, B.W.; Suslick, K.S. Sonochemical synthesis of nanomaterials. *Chem. Soc. Rev.* **2013**, *42*, 2555–2567. [CrossRef]
26. Raj, B.G.S.; Kim, H.-Y.; Kim, B.-S. Ultrasound assisted formation of Mn_2SnO_4 nanocube as electrodes for high performance symmetrical hybrid supercapacitors. *Electrochim. Acta* **2018**, *278*, 93–105.
27. Zhao, B.; Lu, M.; Wang, Z.; Jiao, Z.; Hu, P.; Gao, Q.; Jiang, Y.; Cheng, L. Self-assembly of ultrathin MnO_2/graphene with three-dimension hierarchical structure by ultrasonic-assisted co-precipitation method. *J. Alloy. Compd.* **2016**, *663*, 180–186. [CrossRef]
28. Jimmy, C.Y.; Yu, J.; Ho, W.; Zhang, L. Preparation of highly photocatalytic active nano-sized TiO_2 particles via ultrasonic irradiation. *Chem. Commun.* **2001**, 1942–1943. [CrossRef]
29. Abiraman, T.; Ramanathan, E.; Kavitha, G.; Rengasamy, R.; Balasubramanian, S. Synthesis of chitosan capped copper oxide nanoleaves using high intensity (30 kHz) ultrasound sonication and their application in antifouling coatings. *Ultrason. Sonochem.* **2017**, *34*, 781–791. [CrossRef]
30. Jin, Z.-L.; Kim, N.-H. RAD51 maintains chromosome integrity and mitochondrial distribution during porcine oocyte maturation in vitro. *J. Reprod. Develop.* **2017**, *63*, 489–496. [CrossRef]
31. Rajabi, A.; Ghazali, M.J. Quantitative analyses of TiC nanopowders via mechanical alloying method. *Ceram. Int.* **2017**, *43*, 14233–14243. [CrossRef]

32. Sulaiman, N.; Ghazali, M.J.; Yunas, J.; Rajabi, A.; Majlis, B.Y.; Razali, M. Synthesis and characterization of $CaFe_2O_4$ nanoparticles via co-precipitation and auto-combustion methods. *Ceram. Int.* **2018**, *44*, 46–50. [CrossRef]
33. Chakraborty, S.; Chelli, V.R.; Das, R.K.; Giri, A.S.; Golder, A.K. Bio-mediated silver nanoparticle synthesis: Mechanism and microbial inactivation. *Toxicol. Environ. Chem.* **2017**, *99*, 434–447. [CrossRef]
34. Thi, V.H.T.; Lee, B.-K. Development of multifunctional self-cleaning and UV blocking cotton fabric with modification of photoactive ZnO coating via microwave method. *J. Photochem. Photobiol. A Chem.* **2017**, *338*, 13–22.
35. Ates, E.S.; Unalan, H.E. Zinc oxide nanowire enhanced multifunctional coatings for cotton fabrics. *Thin Solid Films* **2012**, *520*, 4658–4661. [CrossRef]
36. Saffari, J.; Mir, N.; Ghanbari, D.; Khandan-Barani, K.; Hassanabadi, A.; Hosseini-Tabatabaei, M.R. Sonochemical synthesis of Fe_3O_4/ZnO magnetic nanocomposites and their application in photo-catalytic degradation of various organic dyes. *J. Mater. Sci.* **2015**, *26*, 9591–9599.
37. Kai, X.; Tian, K.; Wang, C.; Jiao, L.; Chen, G.; Zhao, Y. Effects of ultrasonic vibration on the microstructure and tensile properties of the nano ZrB_2/2024Al composites synthesized by direct melt reaction. *J. Alloys Compd.* **2016**, *668*, 121–127. [CrossRef]
38. Zeiger, B.W.; Suslick, K.S. Sonofragmentation of molecular crystals. *J. Am. Chem. Soc.* **2011**, *133*, 14530–14533. [CrossRef]
39. Zhang, Z.P.; Rong, M.Z.; Zhang, M.Q.; Yuan, C.E. Alkoxyamine with reduced homolysis temperature and its application in repeated autonomous self-healing of stiff polymers. *Polym. Chem.* **2013**, *4*, 4648–4654. [CrossRef]
40. Jiang, J.; Wan, F.; Yang, J.; Hao, W.; Wang, Y.; Yao, J.; Shao, Z.; Zhang, P.; Chen, J.; Zhou, L. Enhancement of osseointegration of polyethylene terephthalate artificial ligament by coating of silk fibroin and depositing of hydroxyapatite. *Int. J. Nanomed.* **2014**, *9*, 4569. [CrossRef]
41. Li, W.D.; Ding, E.Y. Preparation and characterization of poly (ethylene terephthalate) fabrics treated by blends of cellulose nanocrystals and polyethylene glycol. *J. Appl. Polym. Sci.* **2007**, *105*, 373–378. [CrossRef]
42. Rokade, A.A.; Patil, M.P.; Yoo, S.I.; Lee, W.K.; Park, S.S. Pure green chemical approach for synthesis of Ag_2O nanoparticles. *Green Chem. Lett. Rev.* **2016**, *9*, 216–222. [CrossRef]
43. Tian, Y.; Jiang, L. Wetting: Intrinsically robust hydrophobicity. *Nat. Mater.* **2013**, *12*, 291. [CrossRef]
44. Kim, K.; Lichtenhan, J.D.; Otaigbe, J.U. Facile route to nature inspired hydrophobic surface modification of phosphate glass using polyhedral oligomeric silsesquioxane with improved properties. *Appl. Surf. Sci.* **2018**, *470*, 733–743. [CrossRef]
45. Feng, B.; Weng, J.; Yang, B.; Qu, S.; Zhang, X. Characterization of surface oxide films on titanium and adhesion of osteoblast. *Biomaterials* **2003**, *24*, 4663–4670. [CrossRef]
46. Kim, B.H.; Lee, D.H.; Kim, J.Y.; Shin, D.O.; Jeong, H.Y.; Hong, S.; Yun, J.M.; Koo, C.M.; Lee, H.; Kim, S.O. Mussel-inspired block copolymer lithography for low surface energy materials of teflon, graphene, and gold. *Adv. Mater.* **2011**, *23*, 5618–5622. [CrossRef]
47. Suryaprabha, T.; Sethuraman, M.G. Fabrication of copper-based superhydrophobic self-cleaning antibacterial coating over cotton fabric. *Cellulose* **2017**, *24*, 395–407. [CrossRef]
48. Wang, X.; Wu, H.-F.; Kuang, Q.; Huang, R.-B.; Xie, Z.-X.; Zheng, L.-S. Shape-dependent antibacterial activities of Ag2O polyhedral particles. *Langmuir* **2009**, *26*, 2774–2778. [CrossRef]
49. Liu, B.; Mu, L.; Han, B.; Zhang, J.; Shi, H. Fabrication of TiO_2/Ag_2O heterostructure with enhanced photocatalytic and antibacterial activities under visible light irradiation. *Appl. Surf. Sci.* **2017**, *396*, 1596–1603. [CrossRef]
50. D'alessandro, A.; Nemkov, T.; Hansen, K.C.; Szczepiorkowski, Z.M.; Dumont, L.J. Red blood cell storage in additive solution-7 preserves energy and redox metabolism: A metabolomics approach. *Transfusion* **2015**, *55*, 2955–2966.
51. Syed, M.; Skonberg, C.; Hansen, S.H. Inhibition of ATP synthesis by fenbufen and its conjugated metabolites in rat liver mitochondria. *Toxicol. In Vitro* **2016**, *31*, 23–29. [CrossRef]
52. Lakshmi Prasanna, V.; Vijayaraghavan, R. Insight into the mechanism of antibacterial activity of ZnO: Surface defects mediated reactive oxygen species even in the dark. *Langmuir* **2015**, *31*, 9155–9162. [CrossRef]

53. Allahverdiyev, A.M.; Abamor, E.S.; Bagirova, M.; Rafailovich, M. Antimicrobial effects of TiO_2 and Ag_2O nanoparticles against drug-resistant bacteria and leishmania parasites. *Future Microbiol.* **2011**, *6*, 933–940. [CrossRef]
54. Wang, X.; Li, S.; Yu, H.; Yu, J.; Liu, S. Ag_2O as a New Visible-Light Photocatalyst: Self-Stability and High Photocatalytic Activity. *Chem. Eur. J.* **2011**, *17*, 7777–7780. [CrossRef]